Understanding of the Bridging Sheet Formation of HIV-1 Glycoprotein gp120

Lin-Tai Da,[†] Jun-Min Quan,*[,†] and Yun-Dong Wu*[,†,‡]

Laboratory of Chemical Genomics, Shenzhen Graduate School of Peking University, Shenzhen 518055, China, and Department of Chemistry, The Hong Kong University of Science and Technology, Clear Water Bay, Kowloon, Hong Kong, China

Received: August 23, 2009

As the initial step of the entry of HIV-1 into cells, the interaction of CD4 with gp120 is a central area of concern in HIV-1 biology and intervention studies. CD4 binding induces large conformational changes to gp120, such as the formation of the bridging sheet between the V1/V2 stem and β20/β21. Understanding the dynamic process and the mechanism that leads to the formation of the bridging sheet is important. We have studied the formation of the bridging sheet via extensive molecular dynamics simulations on a modeled intermediate state. The intermediate state is derived from the crystal structure of the gp120/CD4 complex with rotation of the α1 helix and separation of the V1/V2 stem from β20/β21. The molecular dynamics simulations reveal that CD4-bound gp120 leads to the refolding of the bridging sheet but the CD4-free gp120 leads to structures similar to unliganded structures of SIV gp120. The bridging sheet refolds with the S375W mutant, but it does not refold with the W112A and S375W/T257S mutants. Our simulation results are in agreement with experimental observations, and they reveal the importance of the formation of the hydrophobic core to the conformational change of CD4-induced gp120. Other experimental observations, including variations in the binding entropy in different mutants, are also qualitatively reproduced.

Introduction

The entry of human immunodeficiency virus type-1 (HIV-1) into target cells involves several steps. The viral exterior envelope glycoprotein, gp120, first binds to the cell surface receptor, CD4,[1,2] which triggers conformational changes to gp120 to expose or form the binding site for the cellular chemokine coreceptors, CCR5 or CXCR4.[3−9] The further conformational changes to gp120 induced by the co-receptor subsequently promote additional conformational changes in the envelope glycoprotein complex involving gp41, which results in the fusion of the viral and cell membranes.[10−16] As the first step of HIV-1 entry into host cells, the interaction of CD4 with gp120 is a central area of concern to HIV-1 biology and intervention studies.[17−23]

Many studies using various methods, such as mutagenic analyses,[24−28] X-ray crystal structures,[29−36] and thermodynamic studies,[37−40] show that CD4 binding induces remarkable conformational changes in gp120. The large conformational changes are thermodynamically demonstrated by the exceptionally large favorable enthalpy (about −50 kcal/mol) and the large unfavorable entropy (about 40 kcal/mol at 310 K) changes.[38] The crystal structures of gp120 in complexes with CD4 and the recent unliganded crystal structure of SIV gp120 provide details about these large conformational changes.[29,34,41] There are few changes in the outer domain, whereas there are dramatic conformational changes in the inner domain and in the bridging sheet mini domain, which involve reshuffling the location and relative orientation of the α1 helix from the inner domain and the β2/β3 strands from the bridging sheet. The β2/β3 strands are more than 40 Å away from the β20/β21 strands in the unliganded state, but they are closely packed with the β20/β21 strands to form the four-stranded bridging sheet in the CD4-bound state (Figure 1a,b). Given that CD4 has only minor direct contact with the β2/β3 strands and the inner domain in the CD4-bound crystal structure, the underlying mechanism through which CD4 induces the large conformational changes in gp120 remains interesting but elusive.

Several mutagenic studies, seeking potential immunogens for broadly neutralizing antibodies, might shed light on the factors that influence the formation of the bridging sheet. Sodroski and Kwong et al. used a mutagenic approach to stabilize gp120 into the CD4 binding conformation.[39,42−44] A cavity-filling mutation, S375W, increases CD4 and CD4i antibody 17b binding while it eliminates the recognition of gp120 by CD4BS antibodies including the broadly neutralizing antibody b12,[39] whereas the S375W mutant with a second-site mutation, T257S, increases the recognition of gp120 by b12 and retains the stabilization from the CD4 binding.[42] Two mutants have distinct thermodynamic characteristics in binding with CD4. The S375W single mutation has a relatively smaller entropy penalty than do the T257S/S375W double mutations, indicating that subtle changes in the Phe43 cavity might influence the folding process of gp120 upon CD4 binding. On the other hand, Chen et al. generated an unliganded conformation of gp120 by removing the β3−β5 loop connecting the V1/V2 stem and the β-sheet of the inner domain, which did not impede the initial rapid binding step of CD4 but inhibited the slow rearrangement step.[28] All of these experiments highlight that the residues lining the Phe43 cavity play a crucial role in mediating the formation of the bridging sheet.

Many conventional[45−47] and biased[48] molecular dynamics (MD) simulations and essential dynamics analyses[49] have been carried out to study the interactions of gp120 and CD4. These studies provide many insights into the conformational features of gp120 and the stabilization effect of CD4 binding on the structure of gp120. We note that most of the simulations are

* To whom correspondence should be addressed. E-mail: quanjm@szpku.edu.cn (J.-M.Q.); chydwu@ust.hk (Y.-D.W.).
[†] Shenzhen Graduate School of Peking University.
[‡] The Hong Kong University of Science and Technology.

10.1021/jp9081239 CCC: $40.75
Published on Web 10/08/2009

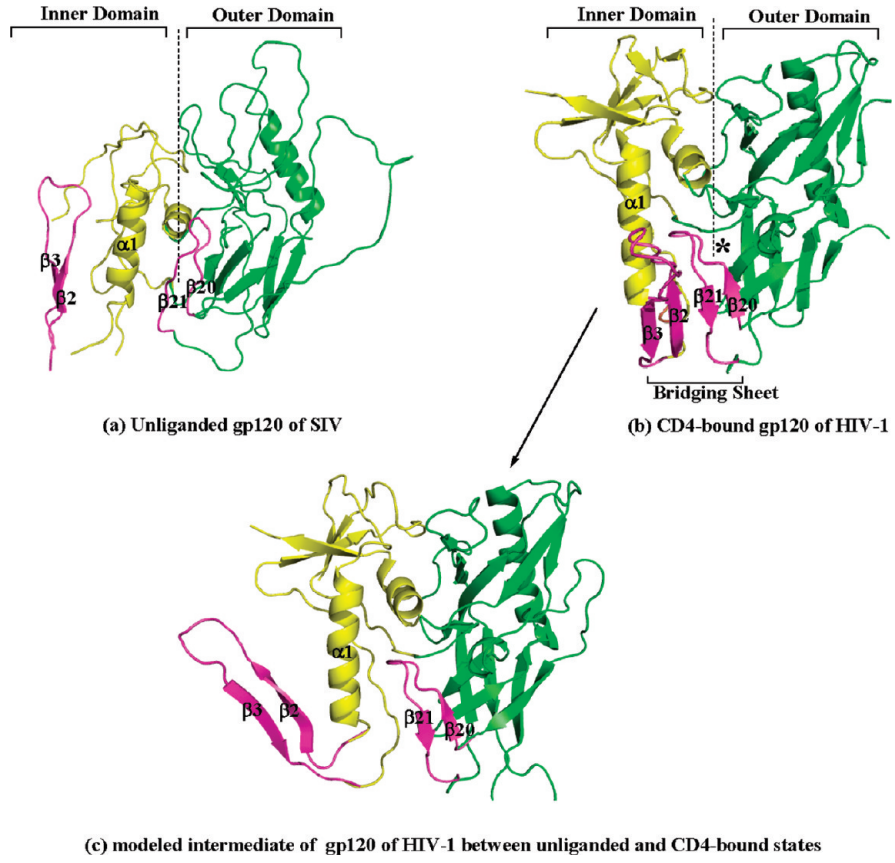

Figure 1. Core structures of unliganded SIV gp120, CD4-bound, and modeled unliganded HIV gp120 (a−c). The unliganded HIV gp120 is modeled from the CD4-bound conformation of gp120 using unliganded SIV gp120 as the structural topology template. The left portion of the core gp120 is the inner domain (yellow), the right portion of the core gp120 is the outer domain (green), and the bottom bridging sheet is highlighted in the CD4-bound gp120. The binding pocket (Phe43 cavity) is indicated by the star symbol, and the boundary between the inner and outer domains is indicated by a black dashed line.

based on the CD4-bound structure of gp120 with a four-stranded bridging sheet and they shed light on the flexibility of the CD4-bound state of gp120 in the presence or absence of CD4, but they did not identify the determinants of the formation of the bridging sheet of gp120 induced by CD4 binding. More experimental and computational studies are therefore needed to elucidate the role of CD4 in the formation of the bridging sheet of gp120.

In this work, we performed extensive MD simulations on the modeled CD4-free and the CD4-bound wild-type gp120, derived from the crystal structure of the gp120-CD4 complex, and three mutants including S375W, T257S/S375W, and W112A. The results show that a separate bridging sheet folds into the four-stranded bridging sheet in the CD4-bound gp120 and S375W mutant, but not in the CD4-free WT gp120. The T257S/S375W and W112A mutations also impede the formation of the bridging sheet. Further analysis reveals that a proper organization of the hydrophobic cluster lining the CD4-binding pocket in the outer domain, induced and stabilized by CD4 or the S375W mutation, is critical for initiating and finalizing the formation of the four-stranded bridging sheet.

Materials and Methods

Generation of the Starting Structures. To study the formation of the four-stranded bridging sheet, we performed MD simulations on the starting structure with a separate bridging sheet. The unliganded HIV gp120 structure is not currently available. Moreover, current conventional MD simulations cannot trace the ab initio formation process that might occur in microseconds to seconds. Therefore, we modeled the HIV gp120 structure with a separate bridging sheet from the CD4-bound HIV gp120 (Figure 1b) by using the unliganded SIV gp120 (Figure 1a) as the structural topology template (Figure 1c). This strategy is based on the fact that the secondary structure is highly conserved between the unliganded SIV and the CD-bound gp120. In addition, the recent cryoelectron tomography of native HIV-1 gp120 trimers indicated that the unliganded HIV-1 gp120 mostly resembles the liganded HIV-1 gp120 except for the V1/V2 loop region.[16]

The starting structures were generated in two stages. In the first stage, the CD4-bound gp120 was derived from the crystal structure in which the gp120 is a core domain in complex with the CD4 D1D2 domain and 17b (PDB entry, 1RZK) by removing 17b.[32] CD4 was truncated to retain only the D1 domain (residues 1−99). The V3 loop was modeled using the crystal structure of a JR-FL strain gp120 as the template (PDB entry, 2B4C).[35] The resulting structure at the first step had a CD4-bound conformation that had a four-stranded bridging sheet and close packing between the inner and outer domains. In the second stage, the outer domain and the $\beta20/\beta21$ strands were fixed with a force (the force constant was equal to 1000 (kJ/mol)/nm^2). The center of mass (COM) of the $\beta2/\beta3$ strands was pulled from the outer domain and the $\beta20/\beta21$ strands by a constant force (force constant equal to 1000 kJ/mol/nm^2). The $\beta2/\beta3$ strands and the inner domain in the final structure had positions and orientations similar to those in the unliganded crystal structure of SIV gp120 in which the bridging sheet is completely separate (Figure 1c). Compared to the less-ordered,

unliganded SIV gp120,[34,50] this modeled structure was more likely to capture a somewhat intermediate state in the folding process. The CD4-free gp120 was generated from the resulting CD4-bound structure by removing the CD4 domain. The S375W, T257S/S375W, and W112A mutants were modeled from the CD4-free WT gp120 structure using SWISS-MODEL.[51]

To examine the artifacts of these modeled structures, we also tried other starting structures, which had different relative orientations of the V1/V2 stem with the outer domain and the inner domain and different structures for the V1/V2 stem itself.

Molecular Dynamics Simulations. All MD simulations were performed with the GROMACS version 3.3.1[52] using the OPLS all-atom force field.[53] Each protein system was immersed in a periodic box with TIP4P water molecules,[54] imposing a minimum solute-wall box distance of 6.5 Å. Suitable numbers of counterions were added to neutralize the system. Long-range electrostatic interactions were treated with the particle-mesh Ewald (PME) summation method.[55] van der Waals and short-range electrostatic interactions were cut off at 1.0 nm. The system was coupled to an external water bath at 310 K with $\tau_T = 0.1$ ps using the Berendsen algorithm[56] and an external pressure reservoir set to 1 bar using weak pressure coupled with $\tau_P = 0.5$ ps. All chemical bonds were constrained using the LINCS algorithm,[57] allowing a time step of 2 fs for the integration of the equation of motion. The pair lists were updated every 10 steps. The solvated system was minimized in 1000 steps of steepest descent minimization, followed by a short 20 ps simulation of the system with position restraints on the protein (force constant equal to 1000 (kJ/mol)/nm^2) to equilibrate the solvents. Before the production simulations, the constraint on the protein was released except for the α1 helix and the V1/V2 stem (β2/β3 strands); 2 ns simulation was then carried out at a temperature of 350 K to accelerate the equilibration of the outer domain and the β20/β21 strands. Finally, 8 ns MD simulation was performed for the resulting system at 310 K without any constraints.

Principal Component Analysis. Principal component analysis (PCA)[58−60] is a convenient method to represent the conformational space explored in an MD trajectory by decreasing the number of variables using multivariate analysis. It uses a covariance matrix, **C**, of the atomic coordinates:

$$C_{ij} = \langle M_{ij}^{1/2}(x_i - \langle x_i \rangle) M_{ij}^{1/2}(x_j - \langle x_j \rangle) \rangle$$

where **M** is a diagonal matrix containing the masses of the atoms (mass-weighted analysis) or the unit matrix (non-mass-weighted analysis) and **C** is a symmetric $3N \times 3N$ matrix. The diagonalization of **C** yields the eigenvectors, R_i, i.e., the principal components and their associated eigenvalues, λ_i. The eigenvalue, λ_i, is the mean square fluctuation of principal component i. The first few principal modes often describe collective global motions in the system.

Configurational Entropy. Configurational entropies were evaluated using Schlitter's[61] procedure, which gives an upper bound approximation to the real configurational entropy, S_{real}, of a molecule based on the mass-weighted covariance matrix of the atom-positional fluctuation that can be calculated from an MD trajectory, where every degree of freedom is treated as a quantum harmonic oscillator. The formula is

$$S_{real} < S = \frac{1}{2} k_B \ln\left\{\det\left[\mathbf{1} + \frac{k_B T e^2}{\hbar^2}\mathbf{M}\boldsymbol{\sigma}\right]\right\}$$

where k_B is Boltzman's constant, T is the absolute temperature, e is Euler's number, $\hbar$ is Plank's constant divided by 2π, **M** is the mass matrix with the masses of the atoms on the diagonal and all off-diagonal elements equal to zero, **1** is the unit matrix, and $\boldsymbol{\sigma}$ is the covariance matrix of atom-positional fluctuations calculated above with the mass-weighted analysis.

The simulations were analyzed using the GROMACS MD package or in-house written codes.

Results and Discussion

CD4 binding induces remarkable conformational changes in gp120 such as the formation of the bridging sheet. We applied a series of MD simulations to explore this dynamic process at the atomic level. The formation of the bridging sheet was monitored by the hydrogen bonds formed between the β20/β21 strands and the β2/β3 strands as depicted in Figure 2. On the basis of the crystal structure of gp120 in complex with CD4, we defined the first hydrogen bond as that formed between the backbones of Cys119 and Met434, and we defined the fifth hydrogen bond as that formed between the backbones of Leu122 and Lys432. The formation of the fifth hydrogen bond indicates the full formation of the bridging sheet.

Dynamics of the CD4-Free and CD4-Bound gp120 in MD Simulations. The MD trajectory of the CD4-free gp120 is significantly different from that of the CD4-bound gp120. The bridging sheet formed readily in the CD4-bound gp120. The first interstrand hydrogen bond was formed at the much earlier stage (about 0.5 ns) in the trajectory, and the other hydrogen bonds were formed subsequently, the last (fifth) hydrogen bond was formed at about 3.0 ns (Figure 2a). These sequential steps were initiated from the packing of W112 from the α1 helix to the docking site that was induced and maintained by CD4 binding. The folding of the four-stranded bridging sheet was also observed in the additional three MD simulations, in which the modeled CD4-bound gp120 had different starting conformations for the V1/V2 (Figures S1−S3 of the Supporting Information). This result suggests that the folding of the modeled gp120 with the separate bridging sheet in the presence of CD4 might not be an artifact.

However, the formation of the bridging sheet was disrupted in the CD4-free gp120, and no interstrand hydrogen bond was formed between the β20/β21 and β2/β3 strands along the 8 ns trajectory (Figure 2b). The β2/β3 strands became a protruding loop from the core domain, which was highly flexible and was captured in multiple conformations. These results suggest that in the intermediate steps of the modeled structure, CD4-bound gp120 with the separate bridging sheet folds back into the four-stranded bridging sheet like that in the CD4-bound crystal structure, whereas CD4-free gp120 with the separate bridging sheet evolves to a more flexible state like that of the unliganded SIV gp120.

The different dynamic behaviors of CD4-free and CD4-bound gp120s were further demonstrated by PCA analysis as shown in Figure 3. The separated β2/β3 strands moved quickly toward the β20/β21 strands and formed the bridging sheet in CD4-bound gp120, and then the CD4-bound conformation remained stable along the whole trajectory, creating a narrow range of spaces. The β2/β3 strands moved away from the β20/β21 strands in the CD4-free gp120, showing highly flexible characteristics.

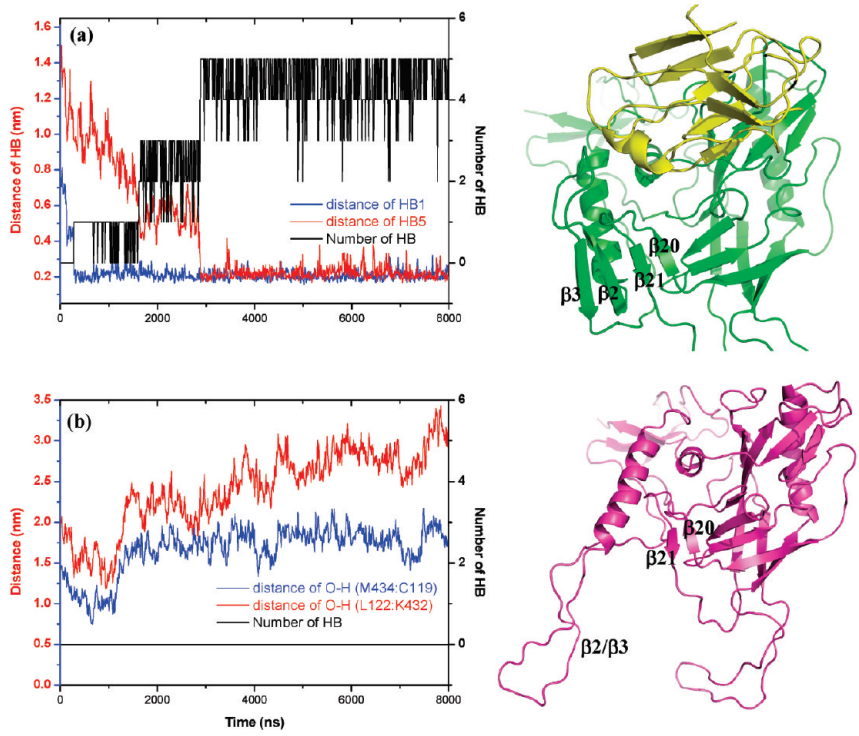

Figure 2. Time evolution of the distances between the hydrogen bonds and the number of hydrogen bonds formed between the $\beta2/\beta3$ strands and the $\beta20/\beta21$ strands in CD4-bound gp120 (a) and CD4-free gp120 (b) in MD simulations. The structures of the final snapshots are shown. The CD4-bound and CD4-free gp120 are shown in green and magenta colors, respectively.

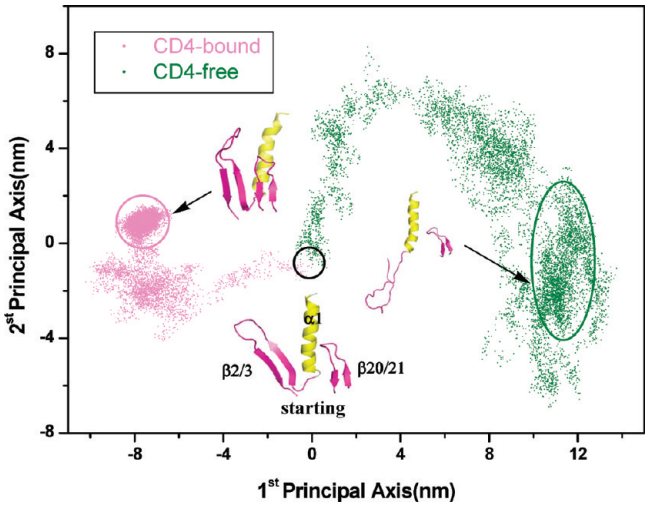

Figure 3. Projections of the trajectories of the CD4-bound and CD4-free gp120s onto the first two principal components. The analyzed regions include the α1 helix and the V1/V2 stem. Each trajectory includes 8000 structures sampled along 8 ns. The conformations sampled at the initial and other stages are denoted by the colored circles. The representative structures are shown in the plot. For clarity, only the α1 helix, $\beta2/\beta3$, and $\beta20/\beta21$ are shown.

These MD results are consistent with experimental observations. Sodroski and co-workers have shown that unliganded gp120 is highly flexible and creates multiple conformational states.[62] CD4 binding induces remarkably large conformational changes to gp120, including the formation of the four-stranded bridging sheet, which corresponds to a large entropy penalty. Our MD simulations explicitly demonstrated these characteristics. The PCA analysis also showed the restriction effects of CD4 on the conformation of gp120 and led to an understanding of the entropy loss from gp120 upon CD4 binding, which is discussed below.

Determinants of the Formation of the Bridging Sheet. To characterize the determinants of the formation of the bridging sheet, we carried out detailed structural analysis of the MD snapshots. After comparing the starting structures of CD4-bound and CD4-free gp120 derived from the 350 K constrained simulations (see Materials and Methods), it is clear that, for the CD4-bound state of gp120 (Figure 4a), a hydrophobic cluster formed by the Phe43 from CD4, the Trp427, Val255, Met475, and the methyl group of Thr257 remain stable throughout the simulation and it provides a partially formed core lining with several other residues, such as Phe382 and Tyr435. This CD4-stabilized partially formed core is suitable for fitting the Trp112 from the adjacent α1 helix observed in the subsequent releasing simulation (Figures 2a and 4a). On the contrary, for the CD4-free gp120, the proper packing within the Trp427, Val255, Met475, and Thr257 residues is destroyed, leading to the collapsed state of Trp427, which blocks the docking site for the Trp112 binding (Figure 4b).

In the following MD simulations, the docking of Trp112 to the partial core can be captured at an early stage in the CD4-bound gp120, which directly drives the formation of the complete hydrophobic core and further facilitates the folding of the V1/V2 stem to form the final bridging sheet. Compared with CD4-bound gp120, in CD4-free gp120, there is no proper environment for Trp112 docking due to the loss of CD4 to stabilize the partial core. In this case, the bridging sheet will not be formed (Figure 2b). Our analysis shows that the proper packing of the α1 helix of the inner domain with the outer domain and the $\beta20/\beta21$ strands is critical for the formation of the four-stranded bridging sheet. Thus, any mutation around this site should have significant impacts on the formation of the bridging sheet. We therefore carried out further MD simulations on three mutants, S375W, T257S/S375W, and W112A, to support this hypothesis.

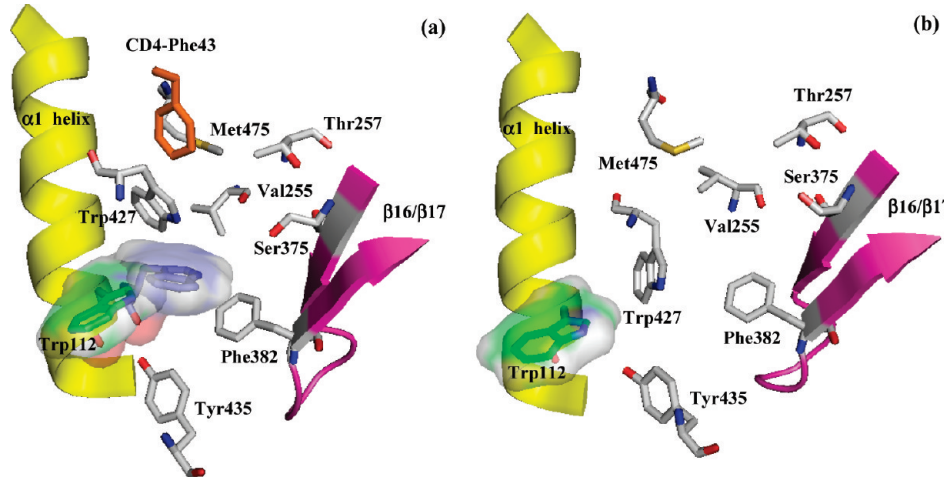

Figure 4. Comparison of the CD4-bound core in the CD4-bound (a) and CD4-free (b) states of gp120. The α1 helix and β16/β17 domains are represented by yellow and pink colors, respectively. The Phe43 from CD4 is colored orange. The carbon atoms of the starting position of Trp112 are in green for both states. The final position of Trp112 along the trajectory in the CD4-bound gp120 is also given with the carbon atoms colored in blue; the surfaces of Trp112 are also given. Other residues in the pocket are shown in silver to indicate the carbon atoms.

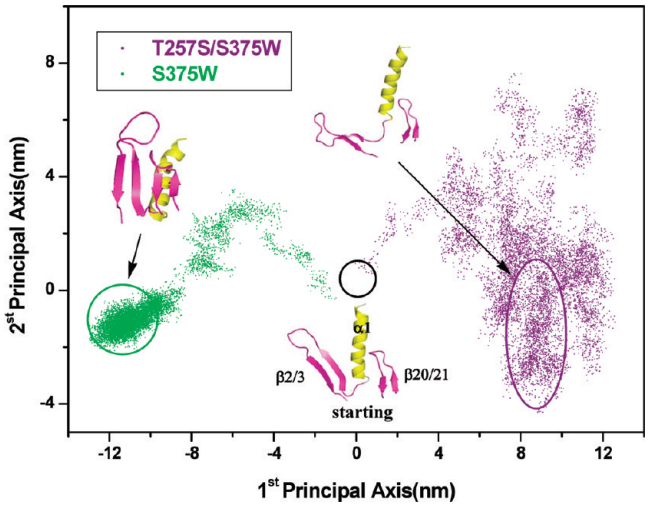

Figure 5. Projections of the trajectories of T257S/S375W and S375W mutant gp120s similar to Figure 3.

Influence of the Cavity-Filling Mutations on the Formation of the Bridging Sheet. Experiments[39,42] have shown that S375W and T257S/S375W have distinct ligand binding phenotypes and they show different thermodynamic changes when gp120 binds with CD4, indicating that these two mutants may have different conformational features in the absence of CD4.

As shown in Figure 5, the S375W and T257S/S375W mutants have quite different conformational spaces along the MD trajectories. The S375W mutant behaves like CD4-bound gp120, forming a four-stranded bridging sheet and creating a relatively narrow conformational space. The trajectory of the T257S/S375W mutant is more like that of the CD4-free gp120, which is highly flexible, and no four-stranded bridging sheet is observed along the 8 ns trajectory.

Inspection of the snapshots of these two mutants shows that the cavity-filling S375W mutation can stabilize the docking site of Trp112 as does Phe43 of CD4, but the deletion of the methyl group of T257 to S257 drives the movement of W375 toward the outer domain and affects the stability of the hydrophobic groove (Figure 6). The flipped V254 partially occupies the docking site of W112. In addition, the more hydrophilic S257 may also influence the stability of the hydrophobic groove. This result gives a qualitative explanation for the experimental observations of the S375W and T257S/S375W mutants.[39,42]

A comparison of the MD structures of the S375W and T257S/S375W mutants and the currently determined crystal structure of b12-bound gp120[63] provides insights into understanding the different ligand binding phenotypes of gp120 mutants. Although the binding site of b12 has many overlaps with the CD4-binding site in the outer domain, the CDR H1 region of the heavy chain of b12 would have a steric clash with the tip of the V1/V2 stem in the CD4-bound conformation of the S375W mutant due to the larger size of b12 compared to the D1 domain of CD4 (Figure 7a). But this steric clash does not occur in the T257S/S375W mutant because the β2/β3 strands are still away from the β20/β21 strands and the outer domain, which explains the higher binding affinity of the T257S/S375W mutant with b12.[63] This result is consistent with the observation that the binding of b12 with gp120 leads to only a low entropy penalty (about 6 kcal/mol),[40] and it also sheds light on the broadly neutralizing capability of b12 against HIV-1 because it does not need to induce large conformational changes in the inner domain and the bridging sheet but prefers a thermodynamically less demanding conformation of gp120.[40,63,64]

Influence of W112A Mutations on the Formation of the Bridging Sheet. The MD trajectories of the CD4-free and CD4-bound gp120, in addition to that of S375W and T257S/S375W, have revealed that the integrity of the docking site of W112 is critical for the formation of the bridging sheet. The importance of the close packing of W112 with its docking site is further highlighted by the MD simulation of the W112A mutant. The separate bridging sheet did not fold in the absence or presence of CD4 (Figures S4 and S5 of the Supporting Information). These results might provide an explanation for the significantly reduced infection capability of the W112A HIV-1 variant,[65] and they also shed light on the weaker binding of the W112A mutant with CD4 and CD4i antibody 17b.[39]

The docking site of W112 might also have overlaps with the potential binding site of BMS-378806, a viral entry inhibitor.[66,67] Both W112A and F382L confer resistance to BMS-378806.[65] On the basis of MD simulations, we propose that BMS-378806 may bind to gp120 to alter the docking site of W112 or directly block the packing of W112 to the docking site and then inhibit the conformational change of gp120 induced by CD4 binding. BMS-378806 binding may not block the formation of an encounter complex of gp120 with CD4, but it might affect the slower and tight binding step and therefore the binding affinity

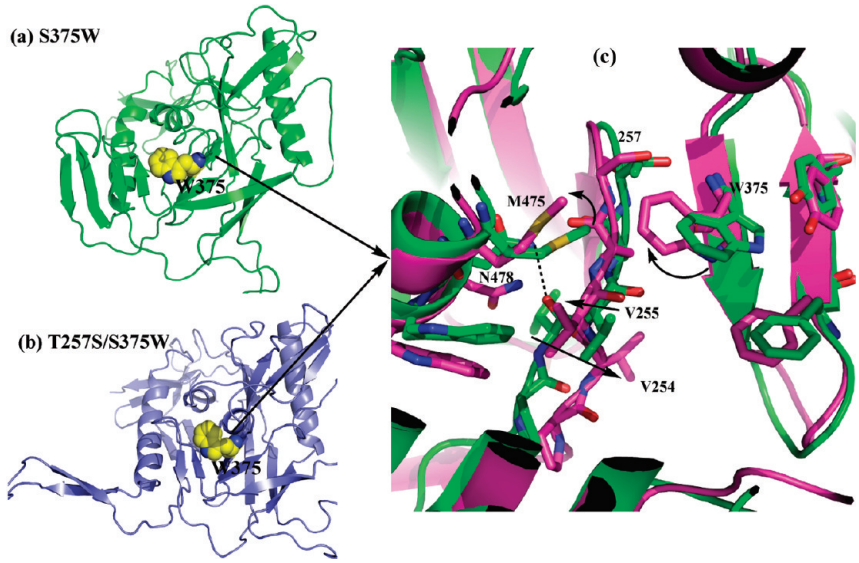

Figure 6. Final snapshots of the S375W (a), T257S/S375W (b), and their superposition structures of the Phe43 cavity (c; green represents S375W and magenta represents T257S/S375W). The hydrogen bond between N478 on the α5 helix and Val254 on the LB is indicated by a dashed line.

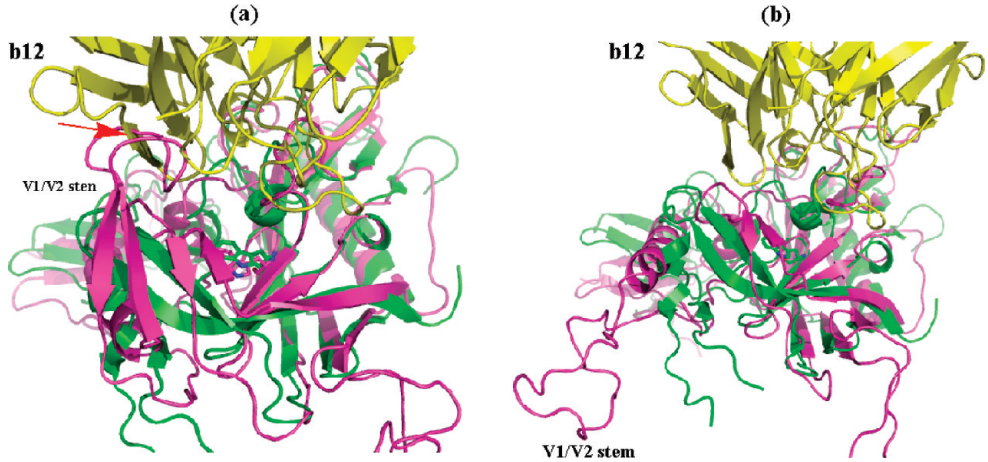

Figure 7. Structural comparison of the b12-bound structure with the MD structures of the S375W mutant and free wild-type gp120. (a) Superposition of the b12-bound structure (green) with the MD structure of S375W mutant gp120 (magenta). The steric clash between the tip of the V1/V2 stem and b12 is indicated by the red-colored arrow. (b) Superposition of the b12-bound structure (green) with the MD structure of the free wild-type gp120 (magenta). b12 is yellow.

of CD4.[28] This proposed mode of action is consistent with the experimental observations that BMS-378806 and its analogues influence CD4 binding and inhibit subsequent downstream entry events.[68]

The proximity of V255, F382, and W427 suggests that the inducement and maintenance of the proper organization of this hydrophobic cluster may not require a large CD4. Much smaller counterparts, such as the cavity-filling W375, can also fulfill a similar function. This analysis is supported by recent discoveries. Mini-protein mimicry of CD4 (CD4M33) can induce structuring of gp120 similar to that induced by CD4.[33] More strikingly, small molecules can also induce conformational changes in gp120 similar to those observed upon CD4 binding.[69,70] This result might provide insight into the design strategies for the surrogates of the covalently cross-linked gp120-CD4 as immunogens.[71−73]

Entropy Change in gp120 upon CD4 Binding. Many thermodynamic experiments have been carried out to characterize the interactions between CD4 and different variants of gp120. Our MD simulations may provide some clues to understanding these data.

We carried out a configurational entropy calculation using Schlitter's formula, which has been used previously to evaluate the entropy of peptides or proteins.[47,74,75] The formation of the bridging sheet is the largest structural change from the CD4-free gp120 to the CD4-bound gp120 in our MD trajectories. It involves the α1 helix of the inner domain, the V1/V2 stem, the β20/β21 strands, and part of the outer domain around the CD4 binding pocket.

We calculated the configurational entropy for this region of gp120 in the CD4-free, CD4-bound, S375W, and T257S/S375W mutants. As shown in Figure 8, in all of the four trajectories, the configurational entropy levels off at the end of the MD trajectories, indicating a relative convergence. As expected, the CD4-free gp120 and the T257S/S375W mutant have relatively larger configurational entropy, whereas CD4-bound gp120 and S375W mutant have reduced configurational entropy. The difference in the configurational entropy between the CD4-free and CD4-bound gp120 is estimated to be about 53.0 ± 1.5 kcal/mol at 310 K. The difference in entropy between the S375W mutant and CD4-bound gp120 is estimated to be about 27.5 ± 3.4 kcal/mol, indicating that the S375W mutant significantly

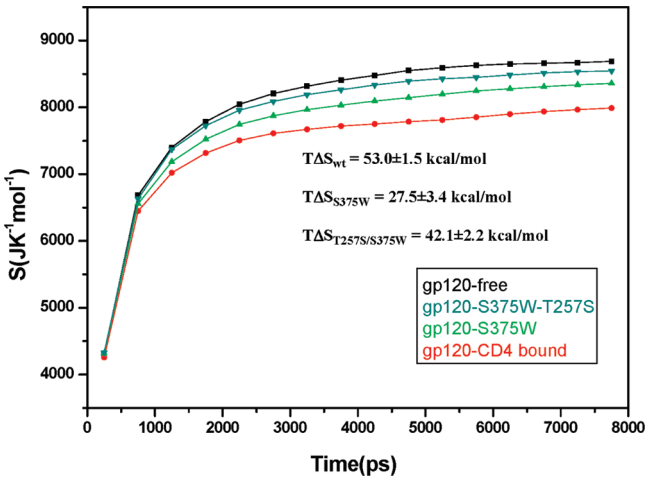

Figure 8. Configurational entropy of the gp120 domain, including the backbone of the α1 helix, V1/V2 stem, β20/β21, LB loop and β9 strand, β15-α3-β16-β17, α5, and the loop linking α5 and the β24 strand.

reduces the entropy upon CD4 binding. On the other hand, the T257S/S375W mutant and CD4-bound gp120 have an entropy difference of about 42.1 ± 2.2 kcal/mol. Thus, the T257S/S375W mutant has a less significant thermodynamic effect than the wide-type gp120 has, but a larger effect than the S375W mutant has.

These results are in good agreement with experimental observations,[38,39,42] and highlight that the formation of the bridging sheet, fixing the α1 helix of the inner domain, the V1/V2 stem, the β20/β21 strands, and part of the outer domain around the CD4 binding pocket, is the main cause of the large entropy change of gp120 binding with CD4.[63]

Meanwhile, our results also help to qualitatively understand experimental observations of other conformationally restrained mutants.[63] Because the formation of the bridging sheet involves the restriction of the α1 helix of the inner domain, the V1/V2 stem, the β20/β21 strands, and part of the outer domain around the CD4 binding pocket, any mutation restricting this region will facilitate the bridging sheet formation process and cause less entropy loss upon CD4 binding. This analysis is consistent with Zhou et al.'s experiments,[63] in which the mutants with a disulfide bond linking the α1 helix of the inner domain and the β20/β21 strands, or linking the β2/β3 strands and β20/β21 strands, has less entropy loss upon CD4 binding compared to the wild-type gp120.

Conclusions

We have characterized the dynamic process of the formation of the bridging sheet in the CD4-bound and S375W mutant gp120 via molecular dynamics simulations. The results demonstrated that a docking site of Trp112, composed of a hydrophobic cluster that lines the CD4-binding pocket, is critical to the formation of the bridging sheet. This docking site is induced and stabilized by CD4 or the cavity-filling S375W mutant, but it collapsed with free wild-type gp120. The formation of the bridging sheet significantly reduces the flexibility of the V1/V2 stem and thus causes the exceptionally large entropy penalty for the free wild-type gp120 upon CD4 binding. In addition, our results provide a plausible explanation for the high potency of the CD4BS antibody b12 against free wild-type gp120 rather than against the S375W mutant.

Acknowledgment. We are very grateful to Dr. Zhixiang Yu for instructive discussion. We gratefully acknowledge financial support for this work from the National Science Foundation of China (Grant 20225312), the Shenzhen municipal "Shuang Bai Project", and the NSFC/RGC Joint Research Project (Grant N_HKUST623/04).

Supporting Information Available: MD simulations of the W112A mutant of gp120, the trajectories from three starting structures of gp120, and complete refs 21, 22, 40, 63, 66, and 68. This material is available free of charge via the Internet at http://pubs.acs.org.

References and Notes

(1) Klatzmann, D.; Champagne, E.; Chamaret, S.; Gruest, J.; Guetard, D.; Hercend, T.; Gluckman, J.-C.; Montagnier, L. *Nature* **1984**, *312*, 767–768.

(2) Dalgleish, A. G.; Beverley, P. C. L.; Clapham, P. R.; Crawford, D. H.; Greaves, M. F.; Weiss, R. A. *Nature* **1984**, *312*, 763–767.

(3) Choe, H.; Farzan, M.; Sun, Y.; Sullivan, N.; Rollins, B.; Ponath, P. D.; Wu, L.; Mackay, C. R.; LaRosa, G.; Newman, W.; Gerard, N.; Gerard, C.; Sodroski, J. *Cell* **1996**, *85*, 1135–1148.

(4) Deng, H.; Liu, R.; Ellmeier, W.; Choe, S.; Unutmaz, D.; Burkhart, M.; Di Marzio, P.; Marmon, S.; Sutton, R. E.; Hill, C. M.; Davis, C. B.; Peiper, S. C.; Schall, T. J.; Littman, D. R.; Landau, N. R. *Nature* **1996**, *381*, 661–666.

(5) Doranz, B. J.; Rucker, J.; Yi, Y.; Smyth, R. J.; Samson, M.; Peiper, S. C.; Parmentier, M.; Collman, R. G.; Doms, R. W. *Cell* **1996**, *85*, 1149–1158.

(6) Feng, Y.; Broder, C. C.; Kennedy, P. E.; Berger, E. A. *Science* **1996**, *272*, 872–877.

(7) Wu, L.; Gerard, N. P.; Wyatt, R.; Choe, H.; Parolin, C.; Ruffing, N.; Borsetti, A.; Cardoso, A. A.; Desjardin, E.; Newman, W.; Gerard, C.; Sodroski, J. *Nature* **1996**, *384*, 179–183.

(8) Trkola, A.; Dragic, T.; Arthos, J.; Binley, J. M.; Olson, W. C.; Allaway, G. P.; Cheng-Mayer, C.; Robinson, J.; Maddon, P. J.; Moore, J. P. *Nature* **1996**, *384*, 184–187.

(9) Forsell, M. N. E.; Dey, B.; Mörner, A.; Svehla, K.; O'dell, S.; Högerkorp, C. M.; Voss, G.; Thorstensson, R.; Shaw, G. M.; Mascola, J. R.; Hedestam, G. B. K.; Wyatt, R. T. *PLoS Pathogens* **2008**, *4*, 1–12.

(10) Sattentau, Q. J.; Moore, J. P. *J. Exp. Med.* **1991**, *174*, 407–415.

(11) Chan, D. C.; Fass, D.; Berger, J. M.; Kim, P. S. *Cell* **1997**, *89*, 263–273.

(12) Tan, K.; Liu, J.; Wang, J.; Shen, S.; Lu, M. *Proc. Natl. Acad. Sci. U. S. A.* **1997**, *94*, 12303–12308.

(13) Weissenhorn, W.; Dessen, A.; Harrison, S. C.; Skehel, J. J.; Wiley, D. C. *Nature* **1997**, *387*, 426–430.

(14) Furuta, R. A.; Wild, C. T.; Weng, Y.; Weiss, C. D. *Nat. Struct. Biol.* **1998**, *5*, 276–279.

(15) Zhu, P.; Liu, J.; Bess, J., Jr.; Chertova, E.; Lifson, J. D.; Grise, H.; Ofek, G. A.; Taylor, K. A.; Roux, K. H. *Nature* **2006**, *441*, 847–852.

(16) Liu, J.; Bartesaghi, A.; Borgnia, M. J.; Sapiro, G.; Subramaniam, S. *Nature* **2008**, *455*, 109–113.

(17) Hussey, R. E.; Richardson, N. E.; Kowalski, M.; Brown, N. R.; Chang, H.-C.; Siliciano, R. F.; Dorfman, T.; Walker, B.; Sodroski, J.; Reinherz, E. L. *Nature* **1988**, *331*, 78–81.

(18) Capon, D. J.; Ward, R. H. R. *Annu. Rev. Immunol.* **1991**, *9*, 649–678.

(19) Moore, J. P.; Burkly, L. C.; Connor, R. I.; Cao, Y.; Tizard, R.; Ho, D. D.; Fisher, R. A. *AIDS Res. Hum. Retroviruses* **1993**, *9*, 529–539.

(20) Jacobson, J. M.; Lowy, I.; Fletcher, C. V.; O'Neill, T. J.; Tran, D. N.; Ketas, T. J.; Trkola, A.; Klotman, M. E.; Maddon, P. J.; Olson, W. C.; Israel, R. J. *J. Infect. Dis.* **2000**, *182*, 326–329.

(21) Burton, D. R.; et al. *Science* **1994**, *266*, 1024–1027 (complete reference given in the Supporting Information).

(22) Lin, P. F.; et al. *Proc. Natl. Acad. Sci. U. S. A.* **2003**, *100*, 11013–11018 (complete reference given in the Supporting Information).

(23) Knight, D.; Weiss, R. A. *Proc. Natl. Acad. Sci. U. S. A.* **2003**, *100*, 10581–10582.

(24) Lasky, L. A.; Nakamura, G.; Smith, D. H.; Fennie, C.; Shimasaki, C.; Patzer, E.; Berman, P.; Gregory, T.; Capon, D. J. *Cell* **1987**, *50*, 975–985.

(25) Cordonnier, A.; Montagnier, L.; Emerman, M. *Nature* **1989**, *340*, 571–574.

(26) Moebius, U.; Clayton, L. K.; Abraham, S.; Harrison, S. C.; Reinherz, E. L. *J. Exp. Med.* **1992**, *176*, 507–517.

(27) Pollard, S. R.; Meier, W.; Chow, P.; Rosa, J. J.; Wiley, D. C. *Proc. Natl. Acad. Sci. U. S. A.* **1991**, *88*, 11320–11324.

(28) Rits-Volloch, S.; Frey, G.; Harrison, S. C.; Chen, B. *EMBO J.* **2006**, *25*, 5026–5036.

(29) Kwong, P. D.; Wyatt, R.; Robinson, J.; Sweet, R. W.; Sodroski, J.; Hendrickson, W. A. *Nature* **1998**, *393*, 648–659.

(30) Wyatt, R.; Kwong, P. D.; Desjardins, E.; Sweet, R. W.; Robinson, J.; Hendrickson, W. A.; Sodroski, J. G. *Nature* **1998**, *393*, 705–711.

(31) Kwong, P. D.; Wyatt, R.; Majeed, S.; Robinson, J.; Sweet, R. W.; Sodroski, J.; Hendrickson, W. A. *Structure Fold. Des.* **2000**, *8*, 1329–1339.

(32) Huang, C. C.; Venturi, M.; Majeed, S.; Moore, M. J.; Phogat, S.; Zhang, M.-Y.; Dimitrov, D. S.; Hendrickson, W. A.; Robinson, J.; Sodroski, J.; Wyatt, R.; Choe, H.; Farzan, M.; Kwong, P. D. *Proc. Natl. Acad. Sci. U. S. A.* **2004**, *101*, 2706–2711.

(33) Huang, C. C.; Stricher, F.; Martin, L.; Decker, J. M.; Majeed, S.; Barthe, P.; Hendrickson, W. A.; Robinson, J.; Roumestand, C.; Sodroski, J.; Wyatt, R.; Shaw, G. M.; Vita, C.; Kwong, P. D. *Structure* **2005**, *13*, 755–768.

(34) Chen, B.; Vogan, E. M.; Gong, H.; Skehel, J. J.; Wiley, D. C.; Harrison, S. C. *Nature* **2005**, *433*, 834–841.

(35) Huang, C. C.; Tang, M.; Zhang, M. Y.; Majeed, S.; Montabana, E.; Stanfield, R. L.; Dimitrov, D. S.; Korber, B.; Sodroski, J.; Wilson, I. A.; Wyatt, R.; Kwong, P. D. *Science* **2005**, *310*, 1025–1028.

(36) Huang, C.-C.; Lam, S. N.; Acharya, P.; Tang, M.; Xiang, S.-H.; Hussan, S. S.; Stanfield, R. L.; Robinson, J.; Sodroski, J.; Wilson, I. A.; Wyatt, R.; Bewley, C. A.; Kwong, P. D. *Science* **2007**, *317*, 1930–1934.

(37) Moore, J. P.; McKeating, J. A.; Weiss, R. A.; Sattentau, Q. J. *Science* **1990**, *250*, 1139–1142.

(38) Myszka, D. G.; Sweet, R. W.; Hensley, P.; Brigham-Burke, M.; Kwong, P. D.; Hendrickson, W. A.; Wyatt, R.; Sodroski, J.; Doyle, M. L. *Proc. Natl. Acad. Sci. U. S. A.* **2000**, *97*, 9026–9031.

(39) Xiang, S. H.; Kwong, P. D.; Gupta, R.; Rizzuto, C. D.; Casper, D. J.; Wyatt, R.; Wang, L. P.; Hendrickson, W. A.; Doyle, M. L.; Sodroski, J. *J. Virol.* **2002**, *76*, 9888–9899.

(40) Kwong, P. D.; et al. *Nature* **2002**, *420*, 678–682 (complete reference given in the Supporting Information).

(41) Kwong, P. D. *Nature.* **2005**, *433*, 815–816.

(42) Dey, B.; Pancera, M.; Svehla, K.; Shu, Y.; Xiang, S._H.; Vainshtein, J.; Li, Y.; Sodroski, J.; Kwong, P. D.; Mascola, J. R.; Wyatt, R. *J. Virol.* **2007**, *81*, 5579–5593.

(43) Dey, B.; Svehla, K.; Xu, L.; Wycuff, D.; Zhou, T. Q.; Voss, G.; Phogat, A.; Chakrabarti, B. K.; Li, Y. X.; Shaw, G.; Kwong, P. D.; Nabel, G. J.; Mascola, J. R.; Wyatt, R. T. *PLoS Pathogens* **2009**, *5*, 1–15.

(44) Mörner, A.; Douagi, I.; Forsell, M. N. E.; Sundling, C.; Dosenovic, P.; O'Dell, S.; Dey, B.; Kwong, P. D.; Voss, G.; Thorstensson, R.; Mascola, J. R.; Wyatt, R. T.; Hedestam, G. B. K. *J. Virol.* **2009**, *83*, 540–551.

(45) Hsu, S. T.; Bonvin, A. M. *Proteins* **2004**, *55*, 582–593.

(46) Pan, Y.; Ma, B.; Keskin, O.; Nussinov, R. *J. Biol. Chem.* **2004**, *279*, 30523–30530.

(47) Hsu, S. T.; Peter, C.; van Gunsteren, W. F.; Bonvin, A. M. *Biophys. J.* **2005**, *88*, 15–24.

(48) Pan, Y.; Ma, B.; Nussinov, R. *J. Mol. Biol.* **2005**, *350*, 514–527.

(49) Liu, S. Q.; Liu, C. Q.; Fu, Y. X. *J. Mol. Graph. Model.* **2007**, *26*, 306–318.

(50) Chen, B.; Vogan, E. M.; Gong, H.; Skehel, J. J.; Wiley, D. C.; Harrison, S. C. *Structure* **2005**, *13*, 197–211.

(51) Schwede, T.; Kopp, J.; Guex, N.; Peitsch, M. C. *Nucleic Acids Res.* **2003**, *31*, 3381–3385.

(52) Lindahl, E.; Hess, B.; van der Spoel, D. *J. Mol. Model.* **2001**, *7*, 306–317.

(53) Price, M. L. P.; Ostrovsky, D.; Jorgensen, W. L. *J. Comput. Chem.* **2001**, *22*, 1340–1352.

(54) Jorgensen, W. L.; Chandrasekhar, J.; Madura, J. D.; Impey, R. W.; Klein, M. L. *J. Chem. Phys.* **1983**, *79*, 926–935.

(55) Essmann, U.; Perera, L.; Berkowitz, M. L.; Darden, T.; Lee, H.; Pedersen, L. G. *J. Chem. Phys.* **1995**, *103*, 8577–8592.

(56) Berendsen, H. J. C.; Postma, J. P. M.; van Gunsteren, W. F.; Di Nola, A.; Haak, J. R. *J. Chem. Phys.* **1984**, *81*, 3684–3690.

(57) Hess, B.; Bekker, H.; Berendsen, H. L. C.; Fraaije, J. G. E. M. *J. Comput. Chem.* **1997**, *18*, 1463–1472.

(58) Garcia, A. E.; Herman, J. G. *Protein Sci.* **1996**, *5*, 62–71.

(59) Hayward, S.; Kitao, A.; Berendsen, H. J. C. *Proteins* **1997**, *27*, 425–437.

(60) Kitao, A.; Hayward, S.; Go, N. *Proteins* **1998**, *33*, 425–437.

(61) Schlitter, J. *Chem. Phys. Lett.* **1993**, *215*, 617–621.

(62) Yuan, W.; Bazick, J.; Sodroski, J. *J. Virol.* **2006**, *80*, 6725–6737.

(63) Zhou, T.; et al. *Nature* **2007**, *445*, 732–737 (complete reference given in the Supporting Information).

(64) Jardetzky, T. *Nature* **2002**, *420*, 623–624.

(65) Madani, N.; Perdigoto, A. L.; Srinivasan, K.; Cox, J. M.; Chruma, J. J.; Lalonde, J.; Head, M.; Smith, A. B.; Sodroski, J. *J. Virol.* **2004**, *78*, 3742–3752.

(66) Wang, T.; et al. *J. Med. Chem.* **2003**, *46*, 4236–4239 (complete reference given in the Supporting Information).

(67) Wang, H. G.; Williams, R. E.; Lin, P. F. *Curr. Pharm. Des.* **2004**, *10*, 1785–1793.

(68) Ho, H. T.; et al. *J. Virol.* **2006**, *80*, 4017–4025 (complete reference given in the Supporting Information).

(69) Schön, A.; Madani, N.; Klein, J. C.; Hubicki, A.; Ng, D.; Yang, X.; Smith, A. B., III.; Sodroski, J.; Freire, E. *Biochemistry* **2006**, *45*, 10973–10980.

(70) Madani, N.; Schon, A.; Princiotto, A. M.; LaLonde, J. M.; Courter, J. R.; Soeta, T.; Ng, D.; Wang, L. P.; Brower, E. T.; Xiang, S. H.; Kwon, Y. D.; Huang, C. C.; Wyatt, R.; Kwong, P. D.; Freire, E.; Smith, A. B., III.; Sodroski, J. *Structure* **2008**, *16*, 1689–1701.

(71) Devico, A.; Silver, A.; Thronon, A. M.; Sarngadharan, M. G.; Pal, R. *Virology* **1996**, *218*, 258–263.

(72) Fouts, T.; Godfrey, K.; Bobb, K.; Montefiori, D.; Hanson, C. V.; Kalyanaraman, V. S.; Devico, A.; Pal, R. *Proc. Natl. Acad. Sci. U. S. A.* **2002**, *99*, 11842–11847.

(73) Devico, A.; Fouts, T.; Lewis, G. K.; Gallo, R. C.; Godfrey, K.; Charurat, M.; Harris, I.; Galmin, L.; Pal, R. *Proc. Natl. Acad. Sci. U. S. A.* **2007**, *104*, 17477–17482.

(74) Schäfer, H.; Daura, X.; Mark, A. E.; van Gunsteren, W. F. *Proteins* **2001**, *43*, 45–56.

(75) Missimer, J. H.; Steinmtz, M. O.; Baron, R.; Winkler, F. K.; Krammerer, R. A.; Daura, X.; van Gunsteren, W. F. *Protein Sci.* **2007**, *16*, 1349–1359.

JP9081239